

TORQUES INDUCED BY SCATTERED PEBBLE-FLOW IN PROTOPLANETARY DISKS

PABLO BENÍTEZ-LLAMBAY¹ AND MARTIN E. PESSAH¹¹*Niels Bohr International Academy, Niels Bohr Institute, Blegdamsvej 17, DK-2100 Copenhagen Ø, Denmark*

ABSTRACT

Fast inward migration of planetary cores is a common problem in the current planet formation paradigm. Even though dust is ubiquitous in protoplanetary disks, its dynamical role in the migration history of planetary embryos has not been assessed. In this Letter, we show that the scattered pebble-flow induced by a low-mass planetary embryo leads to an asymmetric dust-density distribution that is able to exert a net torque. By analyzing a large suite of multifluid hydrodynamical simulations addressing the interaction between the disk and a low-mass planet on a fixed circular orbit, and neglecting dust feedback onto the gas, we identify two different regimes, gas- and gravity-dominated, where the scattered pebble-flow results in almost all cases in positive torques. We collect our measurements in a first torque map for dusty disks, which will enable the incorporation of the effect of dust dynamics on migration into population synthesis models. Depending on the dust drift speed, the dust-to-gas mass ratio/distribution and the embryo mass, the dust-induced torque has the potential to halt inward migration or even induce fast outward migration of planetary cores. We thus anticipate that dust-driven migration could play a dominant role during the formation history of planets. Because dust torques scale with disk metallicity, we propose that dust-driven outward migration may enhance the occurrence of distant giant planets in higher-metallicity systems.

Keywords: protoplanetary disks, planet-disk interactions, planets and satellites: formation, dynamical evolution and stability, gaseous planets, hydrodynamics, scattering, methods: numerical

1. INTRODUCTION

Planetary embryos are born and grow in a protoplanetary disk composed of gas and a small fraction of dust, pebbles and rocky fragments. The gaseous disk exerts a gravitational torque onto the nascent planets that can modify dramatically their orbits (e.g., Kley & Nelson 2012; Baruteau & Masset 2013; Baruteau et al. 2014). Gradients in the density and temperature in the gas disk alter the torques exerted on a planet, but have a mild impact on the so-called differential Lindblad torque (Ward 1997). An additional torque is exerted by the horseshoe orbits around the protoplanet. The torque associated with this so-called horseshoe drag (Ward 1991) can become positive and larger than the differential Lindblad torque if the gradients of vortensity or entropy are strong enough (e.g., Baruteau & Masset 2008; Masset & Casoli 2009; Paardekooper et al. 2010). Typically, the net torque resulting from these contributions is such that inward migration is expected for low-mass embryos (Tanaka et al. 2002).

While it is accepted that migration can be neglected for masses smaller than the mass of Mars ($\sim 0.1 M_{\oplus}$) (Morbidelli & Raymond 2016), it becomes difficult to overcome inward migration for embryos larger than $\sim 1 M_{\oplus}$ on timescales of a few Myr – the lifetime of protoplanetary disks

(e.g. Mamajek 2009). In addition, planet population synthesis studies usually require a reduced migration efficiency in order to produce results consistent with observations (e.g. Cossou et al. 2014). Several mechanisms able to reduce the migration rate have been proposed during the last decade. Some of these are related to torques in non-isothermal disks (e.g. Paardekooper & Mellema 2006; Masset & Casoli 2010; Paardekooper et al. 2010, 2011; Jiménez & Masset 2017), torques in magnetized disks (e.g. Baruteau et al. 2011; Guilet et al. 2013; Uribe et al. 2015), thermal torques (e.g. Lega et al. 2014; Benítez-Llambay et al. 2015; Masset & Velasco Romero 2017; Masset 2017) and torques arising when considering the detailed three-dimensional flow close to the planet (e.g. Fung et al. 2015, 2017). All of these effects rely on modifications to the temperature and density of the gas in the vicinity of the planet.

Whereas the effects of gaseous torques on planetary migration have been the focus of numerous studies, the possibility that dust¹ could play a significant role has been barely considered². This is perhaps not surprising as it is widely accepted that the dust-to-gas ratio is only about $\sim 1\%$ in

¹ Here, *dust* refers to particles that are not directly subject to a dust pressure force but indirectly to the gas pressure by mean of a gas headwind.

² Fouchet et al. (2010) seems to be the only work that has focused on this question. However, they did not find torques due to the dust component, perhaps due to the large planetary mass considered.

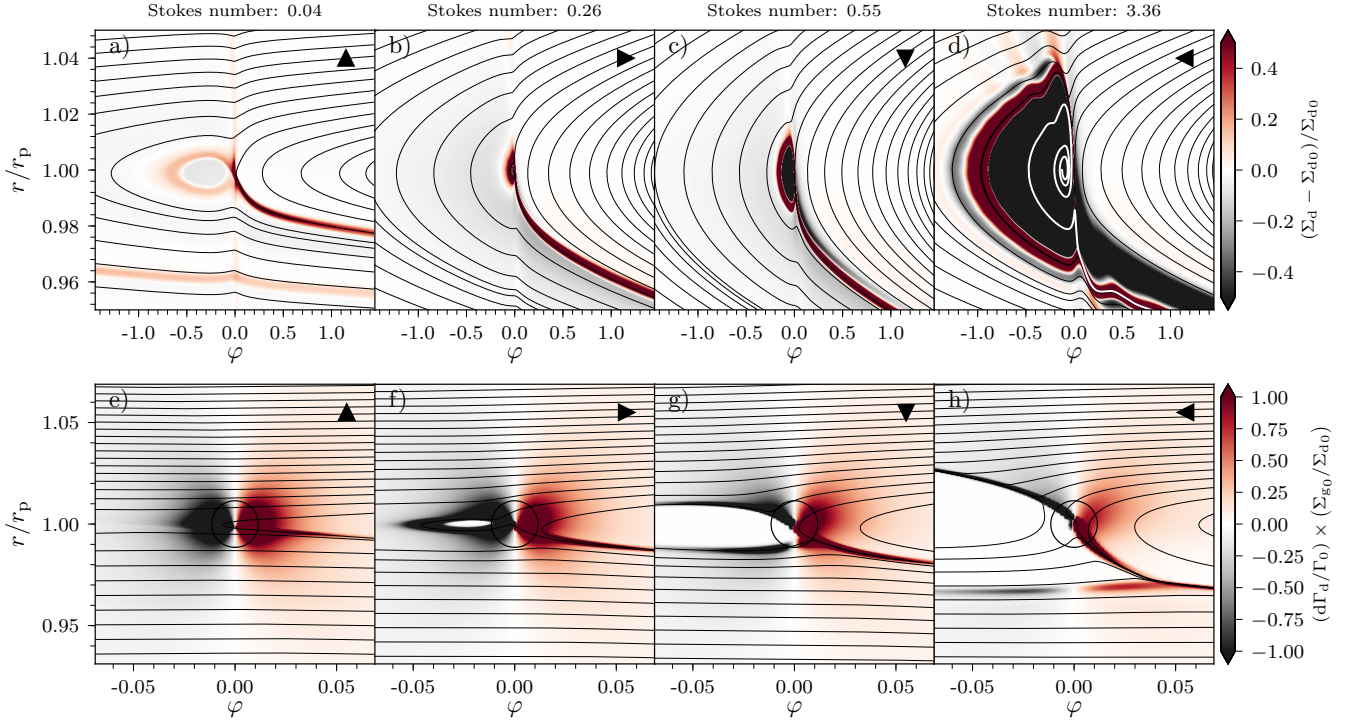


Figure 1. Top: relative dust-density perturbations and dust streamlines (black lines) for four different Stokes numbers, corresponding to the black triangles in Fig. 2. Panel (d) includes a streamline starting inside the dust hole (white line) to illustrate the unstable behavior that leads to its formation. Bottom: associated torque density distribution, $d\Gamma_d$ normalized by $\Gamma_0 = (m_p/M_*)^2 \Sigma_{g0} r_p^4 \Omega_p^2 / h^2$. The black circle corresponds to the Hill radius of the planet. Note the different scales used in each set of panels.

mass, which makes it hard to believe that dust can be dynamically important for migration. In this Letter we show that dust-induced torques can indeed be important because the dust-density distribution around the planet can become significantly asymmetric due to the interplay between the drag force and the scattering by the planet (e.g., Figs. 2–5 in [Morbidelli & Nesvorný 2012](#)). Even though hints of these asymmetries in the dust distribution surrounding the planet have already been observed (e.g., [Dipierro & Laibe 2017](#)), the resulting dust-induced torque has not been recognized and assessed in a systematic way.

We present systematic measurements of the torques produced by the dust component of the disk and show that these are able to alter the migration history of a protoplanet. We show in the upper panel of Fig. 1 how these asymmetries manifest themselves in the flow surrounding the planet. For a wide range of conditions, the associated asymmetric torque density distribution, shown in the lower panel of Fig. 1, leads naturally to a positive dust-induced torque component. By performing a suite of 200 numerical simulations, we find that asymmetries in the scattered dust flow are able to change the magnitude and even the sign of the net torque acting on a planet, and that the value of the dust-induced torque depends on the particles’ size and mass of the planet. In addition, the efficiency of this torque component compared to the gas torque depends on the dust-to-gas mass ratio/distribution. We

summarize our results in a first torque map for dusty disks which we present in Fig. 2.

2. NUMERICAL SIMULATIONS

We perform numerical simulations using the FARGO3D³ code ([Benítez-Llambay & Masset 2016](#)), which solves the equations for fluid dynamics using finite-difference upwind, dimensionally split methods, combined with the FARGO algorithm ([Masset 2000](#)) for the orbital advection and a fifth order Runge-Kutta integrator for planetary orbits. We extended the code to deal with multiple fluids, and treat the dust particles as a pressureless fluid ([Benítez-Llambay et al., in prep](#)).

The basic equations of our model are those given in [Weber et al. \(2018\)](#). We employ a disk model that corresponds to the steady-state solution of an α -disk ([Shakura & Sunyaev 1973](#)). The background density and temperature are power laws in radius with indices $-1/2$ and -1 , respectively. The aspect ratio of the disk is set to $h = 0.05$ and the α -parameter is set to $\alpha = 3 \times 10^{-3}$. For the dust component we adopt the steady-state solution described in [Takeuchi & Lin \(2002\)](#). Because dust feedback is not considered and we parametrize the drag force via the Stokes number, the absolute value for the gas and dust surface densities, Σ_g and Σ_d , respectively,

³ <http://fargo.in2p3.fr>

are not relevant. For the sake of definiteness, we set both to unity. We use a locally isothermal equation of state for the gas.

We implement a non-uniform 2D polar grid radially refined close to the planet according to the mesh density function $\psi(r) = 1/r + \xi/[(r - r_p)^2 + \xi^2]$, where the parameter ξ , taken to be 0.1, sets the relative density of cells close to the planet location r_p , which we consider fixed in a frame rotating with angular frequency Ω_p . The mesh has 768 radial zones in the domain $r \in [0.48, 2.08] r_p$, which results in a cell size of $5 \times 10^{-4} r_p$ at the planet position, allowing us to resolve both the horseshoe orbits of the smallest planet considered, $m_p = 10^{-6} M_*$ (with M_* the stellar mass), and the pressure scale for all the Lindblad resonances far away from the planet. The mesh is azimuthally divided in 3072 uniform sectors. In the cases limited by the dashed line in Fig. 2, we increased the resolution by using 12288 azimuthal zones and setting $\xi = 0.05$, which results in a resolution of $\sim 2.7 \times 10^{-4} r_p/\text{cell}$ at the planet location.

We adopt damping buffer zones (de Val-Borro et al. 2006) for the radial velocity, in rings extending from the inner (outer) boundaries to the radius where the angular frequency of the disk matches $2/3$ ($3/2$) of the angular frequency at the boundary. The damping timescale is chosen equal to 0.3 local orbital periods (Benítez-Llambay et al. 2016). The smoothing length for the planet potential is equal to its Hill radius. We explore the problem by setting a two dimensional, logarithmic grid in the parameter space spanned by the planetary mass and the Stokes number, defining 10 bins in the range $m_p \in [10^{-6}, 3 \times 10^{-5}] M_*$ and 20 in the Stokes number range $[10^{-2}, 10]$. The total integration time is equal to 50 planetary orbits. The majority of the simulations reach steady state long before this time span. A systematic exploration involving hundreds or thousands of orbits at lower resolutions confirms that longer integration times do not alter the torque measurements that we report below.

3. TORQUE MAP FOR DUSTY DISKS

In order to assess the importance of the dust torque compared to the gaseous one, we summarize our measurements in the torque map shown in Fig. 2. We plot the relative strength of the dust torque, Γ_d , to the gas torque, Γ_g , for all of the simulations carried out. The torques were obtained as instantaneous measurements at 50 orbits. This is justified because the values of the torques vary little with respect to their mean.

Valuable insight for understanding the physical processes determining the global morphology of the torque map can be obtained by analyzing the dust dynamics in the vicinity of the planet. With this goal, we show in Fig. 1 the dust surface density perturbation and torque densities for different Stokes number at constant planetary mass. We overlay the dust streamlines, showing the expected horseshoe orbits altered by a strong radial velocity induced by the drag force (cf. Ogilvie & Lubow 2006; Morbidelli & Nesvorný 2012). Particles approaching the planet experience a strong torque, which increases their semi-major axis and eccentricity, a pro-

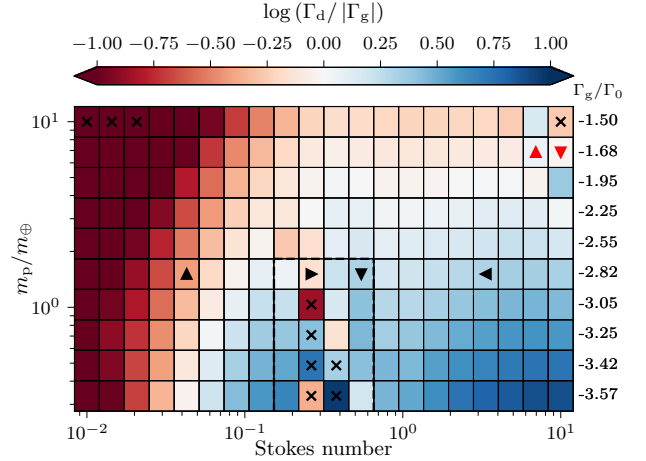


Figure 2. Torque map summarizing the numerical exploration. Positive dust torques are found in the majority of the cases, except those marked with crosses, for which we use the absolute value of the torque. There are two regions where dust torques exceed gas torques, leading to outward migration. For small Stokes numbers (gas-dominated regime) the dust torque is produced by small-scale asymmetries close to the planet. For large Stokes numbers (gravity-dominated regime), the dust torque is due to the dust hole behind the planet. The dust torques were obtained considering a 1% dust-to-gas mass ratio. Numbers to the right provide the gas torque normalized by $\Gamma_0 = (m_p/M_*)^2 \Sigma_{g0} r_p^4 \Omega_p^2 / h^2$. Because the dust torque scales with the dust surface density, for a given dust-mass distribution, the net torque is obtained by direct multiplication by the dust-to-gas ratio per bin. The black (red) triangles correspond to the simulations presented in Fig. 1 (Fig. 3). The rectangle delimited by the dashed line corresponds to high-resolution simulations in the transition region between the gas and gravity-dominated regimes.

cess well captured by the impulse approximation (Lin & Papaloizou 1986).

As the Stokes number increases (from left to right), Fig. 1 displays a clear trend. The drag force decreases and, as expected, the particles experiment larger variations in their orbital elements. In the limit of perfect coupling (Stokes number $\rightarrow 0$), the dust is a perfect tracer of the gas, while in the regime where the dust is dynamically decoupled (Stokes number $\rightarrow \infty$), the particles trace the test particle orbits in the restricted three-body problem. This can clearly be seen by comparing the size of the horseshoe orbits in panels (a) and (d) (see Paardekooper & Papaloizou 2009).

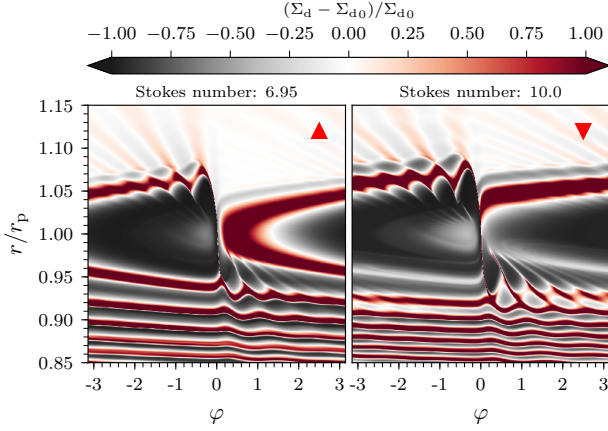


Figure 3. Relative dust surface density for two different Stokes numbers, corresponding to the red triangles in Fig. 2. Left panel: an overdense stream is able to enhance the positive torque when approaching the planet from its front. Right panel: For larger Stokes numbers, this stream is scattered away by the planet, transforming the hole into a gap and, in this case, decreasing the dust-torque.

3.1. Gas and Gravity-dominated Regimes

We identify two different regimes leading to positive dust torques: the *gas-dominated* and *gravity-dominated* regimes, which are connected by a transition regime, in which the dust torque may decrease in magnitude and, for some cases, reverse sign.

Gas-dominated regime (a & e) – Dust scattering is only efficient very close to the planet, accumulating an incident tube of particle streamlines along a ring-shaped overdense stream. In this process the eccentricity of the scattered dust is quickly damped. This overdensity corresponds to the limit of a protected region, which, for the sake of simplicity, we call the *dust hole*. The dust hole is isolated from the incoming beam of particles and, because it is draining out its dust content, it becomes underdense. Because an underdense counterpart does not exist in front of the planet, this enhances the possibility that a positive torque develops. When inspecting the torques close to the planet, a torque dipole is observed as well as two small filaments, the origin of which can be tracked down to a stagnation point located behind the planet. Dust concentrates in a filament that crosses the Hill radius of the planet. Interestingly, this asymmetry produces a positive torque, a robust result to variations in the planet mass and the Stokes number. We find the dust torques arising in this region of parameter space to be positive and gradually increasing with Stokes number. In addition, its ratio to the gaseous torque decreases with planetary mass. As the Stokes number increases further, the dust hole shrinks and, for very low-mass planets, it may eventually close, leading to the transition regime. We note that in the small Stokes number regime, it may be possible to gain insight into the dynamical processes determining the dust torque by employing the formalism introduced in Lin & Youdin (2017).

Transition regime (b & f) – As the Stokes number increases (resulting in weaker drag), the hole develops and expands. The interplay between the scattered dust flow induced by the planet and the drag force produced by the aerodynamic friction with the gas effectively generates a barrier. Particles arriving from the ambient flow cannot enter while dissipative forces expel those inside. This is illustrated by the white streamline in panel (d) of Fig. 1. While the drift speed increases, the drag force remains large enough so as to prevent efficient scattering to occur and the dust tends to accumulate behind and closer to the planet. The dust overdensity behind the planet now competes against the overdense filament in front of the planet, effectively reducing the net dust torque. As the Stokes number increases further, the overdense lobe behind the planet rapidly expands leading to an abrupt, but continuous, transition into the gravity-dominated regime. Depending on the mass of the planet, this can reduce the positive torque and even change its sign. When inspecting the torque distribution, we observe that small planets seem to be unable to open a hole in order to reduce the excess of negative torque, leading to a net negative dust torque. In general, the less massive the planet, the more negative the torque can become. We find that, depending on the mass of the planet, the value of the torque in this regime can be very sensitive to the dust distribution close to the planet and the shape of the hole. As the hole seems to be absent, or is very tiny for small planets, very high resolution is imperative in order to correctly resolve this regime. For larger Stokes numbers, the hole continues expanding both radially and azimuthally, and the dust torque enters the gravity-dominated regime.

Gravity dominated regime (c & g)-(d & h) – This regime is characterized by significant changes in the dust dynamics, in which the semi-width of the horseshoe orbits is modified from $\sim r_p \sqrt{m_p/(hM_\star)}$ to $\sim 2.5r_p \sqrt[3]{m_p/(3M_\star)}$ (Paardekooper & Papaloizou 2009), as well as a change in the dust drift speed. For larger Stokes numbers (d), depending on the mass of the planet, epicyclic motion starts to be evident. Naturally, because there exists a hole behind the planet and an overdense stream ahead of it, the net torque becomes positive. The larger the Stokes number is, the larger the azimuthal size of the hole becomes, providing a natural scaling for the torque with the Stokes number. The general picture, however, is not simple. For example, while the size of the hole increases, because the disk is azimuthally periodic the overdense stream approaches the planet from the front, thus enhancing the torque. This feature is observed for intermediate masses and large Stokes numbers, as shown in the left panel of Fig. 3. For large planet masses and Stokes numbers, the planet perturbations are such that a dust particle is not able to drift before it gets scattered again by the planet, creating a dust barrier that leads to the formation of a gap in the dust component. This kind of configuration is shown in the right panel of Fig. 3. It is worth noticing that the physical processes responsible for producing the dust torque in this regime are similar to those driving type-III migration (e.g. Masset & Papaloizou 2003; Pepliński et al. 2008). The underdense dust hole is analogous to the *gas mass deficit* in the

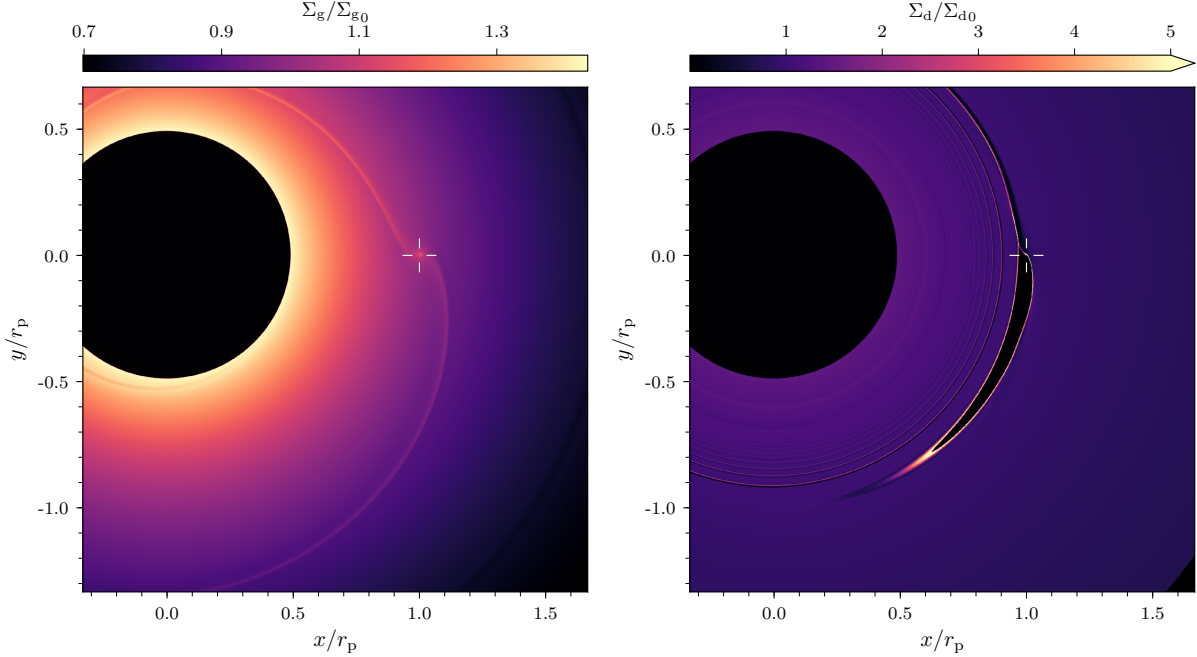


Figure 4. Cartesian representation of the gas and dust surface density corresponding to the simulation presented in panel (d) in Fig. 1. The white crosshair marks the planet’s position.

co-orbital region in type-III migration. In both of these cases, the size and shape of the mass deficit depends on the planet mass and the drift speed. We thus anticipate that the concepts developed in the framework of type-III migration could be adapted to investigate the dynamical processes shaping the dust hole. We illustrate the gas and dust surface densities in Cartesian coordinates for one of our simulations in Fig. 4.

It is worth noticing that there exist similarities between our findings and those presented by Capobianco et al. (2011), who investigated the potential for planetesimals to alter the migration history of small mass cores embedded in a gaseous disk. In order to investigate this so-called planetesimal-driven migration, their study, based on the N-body approach, focuses on the (cumulative effects of the) torque exerted by close encounters subject to a simple aerodynamic model. This is related, but different, to our approach. Here, we consider the torque exerted by the whole dust distribution in steady state taking into account the gas dynamics. This makes it possible for us to assess the net effect in terms of the resulting global asymmetry in the dust surface density. Nevertheless, Capobianco et al. (2011) also found that planetesimal-driven outward migration is possible for small mass planets. In spite of the different scales and approaches involved in studying these two problems, this seems to be an indication that the mechanisms involved share important similarities. This calls for further investigation in order to establish any potential connections on solid grounds.

3.2. Assessment of the Robustness of our Findings

The precise value obtained when measuring the dust torque is sensitive to the smoothing length. As the smoothing nec-

essary to produce results comparable to a 3D simulation (which is probably sensitive to the dust distribution in the vertical direction and the Stokes number) is not known, we adopted a smoothing length that scales with the quantity that seems to be dynamically relevant for dust, i.e., the Hill radius. We note, however, that the effective smoothing in the gas-dominated regime may be larger. This is because in the well-coupled regime, the smoothing length should tend toward that of the gas component ($\epsilon/r_p = 0.6h$, Müller et al. (2012)). We have checked that measuring the torque with different smoothing lengths does not alter significantly the trends presented in Fig. 2. In particular, the dust torque in the gravity-dominated regime is very robust, because it arises from a large-scale asymmetry. This is, however, not necessarily the case in the gas-dominated regime, where the dust torque results from a more subtle asymmetry close to the planet. In order to minimize spurious measurements due to unresolved dynamics, we have conservatively cut off the inner half of the Hill sphere when computing torques. A more thorough assessment of the robustness of our results will require 3D high-resolution simulations, where the smoothing length is not a free parameter.

The surface density profile has an impact on the gaseous corotation torque (e.g., Tanaka et al. 2002), which is usually a positive quantity and vanishes for surface density profiles $\propto r^{-3/2}$. This contribution makes the total gas torque less negative, thus enabling the dust torque to slow down or even reverting the migration (Paardekooper et al. 2010). We have used $\Sigma_g \propto r^{-1}$, which leads to a rather conservative corotation torque. We anticipate that the effect we describe is prone

to be enhanced in more realistic disks, where the corotation torque may increase considerably.

We have modeled the dust as a pressureless fluid. This approach may break down when the dynamics is governed by crossing orbits in low-density regions. In this regime, further studies employing Lagrangian particles are necessary to ultimately validate our findings. It is worth mentioning, however, that the streamlines characterizing the dust dynamics in our models share many key properties with those presented using particles (e.g., [Morbiddelli & Nesvorny 2012](#)).

4. FUTURE WORK AND IMPLICATIONS

In this Letter, we have provided a first assessment of the potential role of dust dynamics on the migration history of low mass planetary embryos. We have identified asymmetries in the dust-density distribution in the vicinity of the planet orbit that may play an important role in determining the net torque on the planet (Fig. 1). We have carried out systematic measurements of these torques and summarized the outcome of our study in a torque map (Fig. 2). This will be useful for incorporating the effect of dust dynamics on migration into planet population synthesis models. We briefly discuss below avenues for future developments and some of the potential implications of our findings.

The efficiency of the dust torque is determined by the relative flow between the dust and the planetary embryo. There are several processes, which we have not considered in this first work, that may play a significant role in more refined models of the early evolution of planetary cores. In particular, future models should account for dust feedback, accretion onto the planetary embryo, planetary migration, and the influence of other planets. We also note that the dust torque in the gas-dominated regime is likely to be sensitive to the gaseous equation of state, because of its impact on the gas flow in the vicinity of the planet. Further studies are necessary in order to quantify and assess the robustness of dust torques in this regime under such modifications.

The strong asymmetries in the dust distribution will alter the opacity of the gas and thus its thermal structure close to the planet. This may have an impact on the thermal torques (e.g. [Lega et al. 2014](#); [Benítez-Llambay et al. 2015](#); [Masset](#)

[2017](#)). Building a unified picture of the migration history of low-mass planets will require modeling dust dynamics, accretion, and thermodynamics self-consistently (e.g., [Chrenko et al. 2017](#)).

The dust torque scales with the dust-mass content, which in addition scales with the metallicity of the disk. Therefore, we predict that outward migration of low-mass embryos is likely to be more effective in systems with higher-metallicity, enhancing the occurrence of distant giant planet in higher metallicity systems.

In order to fully assess the role of dust torques on planet migration it is necessary to consider realistic dust-size/mass distributions. Nevertheless, the dust torque seems a good candidate for slowing down or even revert the migration of low-mass planetary cores. We thus anticipate that dust-driven migration could play a dominant role during the formation history of planets, including those in our own Solar System.

We thank the anonymous referee for a timely and constructive report, which helped us improve the manuscript. We thank Leonardo Krapp, Alejandro Benítez-Llambay & Ximena Ramos for useful discussions and Frederic Masset, Tobias Heinemann and Oliver Gressel for useful comments. We thank Colin McNally for his valuable input based on a preprint version of this Letter. This project has received funding from the European Union’s Horizon 2020 research and innovation programme under grant agreement No. 748544. The research leading to these results has received funding from the European Research Council (ERC) under the European Union’s Seventh Framework programme (FP/2007-2013) under ERC grant agreement No. 306614 and under the European Union’s Horizon 2020 research and innovation programme (grant agreement No 638596). This work was supported by a research grant (VKR023406) from VIL-LUM FONDEN. We acknowledge PRACE for awarding us access to MareNostrum at Barcelona Supercomputing Center (BSC), Spain. Computations were performed at the HPC center of the University of Copenhagen.

Software: IPython ([Pérez & Granger 2007](#)), NumPy ([Walt et al. 2011](#)), Matplotlib ([Hunter 2007](#))

REFERENCES

- Baruteau, C., Fromang, S., Nelson, R., & Masset, F. 2011, *A&A*, 533, A84
- Baruteau, C., & Masset, F. 2008, *ApJ*, 672, 1054
- Baruteau, C., & Masset, F. 2013, in *Lecture Notes in Physics*, Berlin Springer Verlag, Vol. 861, 201
- Baruteau, C., Crida, A., Paardekooper, S.-J., et al. 2014, *Protostars and Planets VI*, 667
- Benítez-Llambay, P., Masset, F., Koenigsberger, G., & Szulágyi, J. 2015, *nat*, 520, 63
- Benítez-Llambay, P., & Masset, F. S. 2016, *ApJS*, 223, 11
- Benítez-Llambay, P., Ramos, X. S., Beaugé, C., & Masset, F. S. 2016, *ApJ*, 826, 13
- Capobianco, C. C., Duncan, M., & Levison, H. F. 2011, *Icarus*, 211, 819
- Chrenko, O., Brož, M., & Lambrechts, M. 2017, *A&A*, 606, A114
- Cossou, C., Raymond, S., Hersant, F., & Pierens, A. 2014, *A&A*, 569, A56
- de Val-Borro, M., Edgar, R., Artymowicz, P., et al. 2006, *MNRAS*, 370, 529
- Dipierro, G., & Laibe, G. 2017, *MNRAS*, 469, 1932

- Fouchet, L., Gonzalez, J.-F., & Maddison, S. T. 2010, *A&A*, 518, A16
- Fung, J., Artymowicz, P., & Wu, Y. 2015, *ApJ*, 811, 101
- Fung, J., Masset, F., Lega, E., & Velasco, D. 2017, *AJ*, 153, 124
- Guilet, J., Baruteau, C., & Papaloizou, J. 2013, *MNRAS*, 430, 1764
- Hunter, J. D. 2007, *Computing In Science & Engineering*, 9, 90
- Jiménez, M. A., & Masset, F. S. 2017, *MNRAS*, 471, 4917
- Kley, W., & Nelson, R. 2012, *ARA&A*, 50, 211
- Lega, E., Crida, A., Bitsch, B., & Morbidelli, A. 2014, *MNRAS*, 440, 683
- Lin, D. N. C., & Papaloizou, J. 1986, *ApJ*, 309, 846
- Lin, M.-K., & Youdin, A. N. 2017, *ApJ*, 849, 129
- Mamajek, E. 2009, in *American Institute of Physics Conference Series*, Vol. 1158, American Institute of Physics Conference Series, ed. T. Usuda, M. Tamura, & M. Ishii, 3–10
- Masset, F. 2000, *A&AS*, 141, 165
- Masset, F., & Casoli, J. 2010, *ApJ*, 723, 1393
- Masset, F., & Papaloizou, J. 2003, *ApJ*, 588, 494
- Masset, F. S. 2017, *MNRAS*, 472, 4204
- Masset, F. S., & Casoli, J. 2009, *ApJ*, 703, 857
- Masset, F. S., & Velasco Romero, D. A. 2017, *MNRAS*, 465, 3175
- Morbidelli, A., & Nesvorný, D. 2012, *A&A*, 546, A18
- Morbidelli, A., & Raymond, S. N. 2016, *Journal of Geophysical Research (Planets)*, 121, 1962
- Müller, T. W. A., Kley, W., & Meru, F. 2012, *A&A*, 541, A123
- Ogilvie, G. I., & Lubow, S. H. 2006, *MNRAS*, 370, 784
- Paardekooper, S.-J., Baruteau, C., Crida, A., & Kley, W. 2010, *MNRAS*, 401, 1950
- Paardekooper, S.-J., Baruteau, C., & Kley, W. 2011, *MNRAS*, 410, 293
- Paardekooper, S.-J., & Mellema, G. 2006, *A&A*, 459, L17
- Paardekooper, S.-J., & Papaloizou, J. C. B. 2009, *MNRAS*, 394, 2297
- Pepliński, A., Artymowicz, P., & Mellema, G. 2008, *MNRAS*, 386, 164
- Pérez, F., & Granger, B. E. 2007, *Computing in Science and Engineering*, 9, 21
- Shakura, N., & Sunyaev, R. 1973, *A&A*, 24, 337
- Takeuchi, T., & Lin, D. N. C. 2002, *ApJ*, 581, 1344
- Tanaka, H., Takeuchi, T., & Ward, W. R. 2002, *ApJ*, 565, 1257
- Uribe, A., Bans, A., & Königl, A. 2015, *ApJ*, 802, 54
- Walt, S. v. d., Colbert, S. C., & Varoquaux, G. 2011, *Computing in Science and Engg.*, 13, 22
- Ward, W. 1991, in *Lunar and Planetary Science Conference*, Vol. 22, Lunar and Planetary Science Conference, 1463
- Ward, W. R. 1997, *Icarus*, 126, 261
- Weber, P., Benítez-Llambay, P., Gressel, O., Krapp, L., & Pessah, M. 2018, *ApJ*, 854, 153